CLEO CONF 97-13
EPS Abstract #332

Observation of Inclusive $B \to \eta^{'} X_s$ Decays

CLEO Collaboration
(August 13, 1997)

Abstract

Using data collected with the CLEO II detector at the Cornell Electron Storage Ring, we report the first observation of high momentum $B \to \eta^{'} X$ transitions. We observe 39.0 ± 10.3 B decay events with $2.0 < P_{\eta^{'}} < 2.7$ GeV/c, the high momentum region where background from $b \to c$ processes is suppressed. We discuss the physical interpretation of the signal, including the possibility that it is due to $b \to s$ gluon transitions. Given that interpretation, We find $\mathcal{B}(B \to \eta^{'} X_s) = (6.2 \pm 1.6(stat) \pm 1.3(sys)) \times 10^{-4}$ for $2.0 < p_{\eta^{'}} < 2.7$ GeV/c.

Typeset using REVTEX

D. M. Asner,[1] J. Gronberg,[1] T. S. Hill,[1] D. J. Lange,[1] S. Menary,[1] R. J. Morrison,[1]
H. N. Nelson,[1] T. K. Nelson,[1] C. Qiao,[1] J. D. Richman,[1] D. Roberts,[1] A. Ryd,[1]
M. S. Witherell,[1] R. Balest,[2] B. H. Behrens,[2] W. T. Ford,[2] H. Park,[2] J. Roy,[2] J. G. Smith,[2]
J. P. Alexander,[3] C. Bebek,[3] B. E. Berger,[3] K. Berkelman,[3] K. Bloom,[3] D. G. Cassel,[3]
H. A. Cho,[3] D. S. Crowcroft,[3] M. Dickson,[3] P. S. Drell,[3] K. M. Ecklund,[3] R. Ehrlich,[3]
A. D. Foland,[3] P. Gaidarev,[3] L. Gibbons,[3] B. Gittelman,[3] S. W. Gray,[3] D. L. Hartill,[3]
B. K. Heltsley,[3] P. I. Hopman,[3] J. Kandaswamy,[3] P. C. Kim,[3] D. L. Kreinick,[3] T. Lee,[3]
Y. Liu,[3] G. S. Ludwig,[3] N. B. Mistry,[3] C. R. Ng,[3] E. Nordberg,[3] M. Ogg,[3,1]
J. R. Patterson,[3] D. Peterson,[3] D. Riley,[3] A. Soffer,[3] B. Valant-Spaight,[3] C. Ward,[3]
M. Athanas,[4] P. Avery,[4] C. D. Jones,[4] M. Lohner,[4] C. Prescott,[4] J. Yelton,[4] J. Zheng,[4]
G. Brandenburg,[5] R. A. Briere,[5] A. Ershov,[5] Y. S. Gao,[5] D. Y.-J. Kim,[5] R. Wilson,[5]
H. Yamamoto,[5] T. E. Browder,[6] Y. Li,[6] J. L. Rodriguez,[6] T. Bergfeld,[7] B. I. Eisenstein,[7]
J. Ernst,[7] G. E. Gladding,[7] G. D. Gollin,[7] R. M. Hans,[7] E. Johnson,[7] I. Karliner,[7]
M. A. Marsh,[7] M. Palmer,[7] M. Selen,[7] J. J. Thaler,[7] K. W. Edwards,[8] A. Bellerive,[9]
R. Janicek,[9] D. B. MacFarlane,[9] P. M. Patel,[9] A. J. Sadoff,[10] R. Ammar,[11] P. Baringer,[11]
A. Bean,[11] D. Besson,[11] D. Coppage,[11] C. Darling,[11] R. Davis,[11] N. Hancock,[11] S. Kotov,[11]
I. Kravchenko,[11] N. Kwak,[11] S. Anderson,[12] Y. Kubota,[12] S. J. Lee,[12] J. J. O'Neill,[12]
S. Patton,[12] R. Poling,[12] T. Riehle,[12] V. Savinov,[12] A. Smith,[12] M. S. Alam,[13] S. B. Athar,[13]
Z. Ling,[13] A. H. Mahmood,[13] H. Severini,[13] S. Timm,[13] F. Wappler,[13] A. Anastassov,[14]
J. E. Duboscq,[14] D. Fujino,[14,2] K. K. Gan,[14] T. Hart,[14] D. Homoelle,[14] K. Honscheid,[14]
H. Kagan,[14] R. Kass,[14] J. Lee,[14] M. B. Spencer,[14] M. Sung,[14] A. Undrus,[14,3] R. Wanke,[14]
A. Wolf,[14] M. M. Zoeller,[14] B. Nemati,[15] S. J. Richichi,[15] W. R. Ross,[15] P. Skubic,[15]
M. Bishai,[16] J. Fast,[16] J. W. Hinson,[16] N. Menon,[16] D. H. Miller,[16] E. I. Shibata,[16]
I. P. J. Shipsey,[16] M. Yurko,[16] S. Glenn,[17] S. D. Johnson,[17] Y. Kwon,[17,4] S. Roberts,[17]
E. H. Thorndike,[17] C. P. Jessop,[18] K. Lingel,[18] H. Marsiske,[18] M. L. Perl,[18] D. Ugolini,[18]
R. Wang,[18] X. Zhou,[18] T. E. Coan,[19] V. Fadeyev,[19] I. Korolkov,[19] Y. Maravin,[19]
I. Narsky,[19] V. Shelkov,[19] J. Staeck,[19] R. Stroynowski,[19] I. Volobouev,[19] J. Ye,[19]
M. Artuso,[20] A. Efimov,[20] M. Goldberg,[20] D. He,[20] S. Kopp,[20] G. C. Moneti,[20]
R. Mountain,[20] S. Schuh,[20] T. Skwarnicki,[20] S. Stone,[20] G. Viehhauser,[20] X. Xing,[20]
J. Bartelt,[21] S. E. Csorna,[21] V. Jain,[21,5] K. W. McLean,[21] S. Marka,[21] R. Godang,[22]
K. Kinoshita,[22] I. C. Lai,[22] P. Pomianowski,[22] S. Schrenk,[22] G. Bonvicini,[23] D. Cinabro,[23]
R. Greene,[23] L. P. Perera,[23] G. J. Zhou,[23] B. Barish,[24] M. Chadha,[24] S. Chan,[24] G. Eigen,[24]
J. S. Miller,[24] C. O'Grady,[24] M. Schmidtler,[24] J. Urheim,[24] A. J. Weinstein,[24]
F. Würthwein,[24] D. W. Bliss,[25] G. Masek,[25] H. P. Paar,[25] S. Prell,[25] and V. Sharma[25]

[1]Permanent address: University of Texas, Austin TX 78712

[2]Permanent address: Lawrence Livermore National Laboratory, Livermore, CA 94551.

[3]Permanent address: BINP, RU-630090 Novosibirsk, Russia.

[4]Permanent address: Yonsei University, Seoul 120-749, Korea.

[5]Permanent address: Brookhaven National Laboratory, Upton, NY 11973.

[1]University of California, Santa Barbara, California 93106
[2]University of Colorado, Boulder, Colorado 80309-0390
[3]Cornell University, Ithaca, New York 14853
[4]University of Florida, Gainesville, Florida 32611
[5]Harvard University, Cambridge, Massachusetts 02138
[6]University of Hawaii at Manoa, Honolulu, Hawaii 96822
[7]University of Illinois, Champaign-Urbana, Illinois 61801
[8]Carleton University, Ottawa, Ontario, Canada K1S 5B6
and the Institute of Particle Physics, Canada
[9]McGill University, Montréal, Québec, Canada H3A 2T8
and the Institute of Particle Physics, Canada
[10]Ithaca College, Ithaca, New York 14850
[11]University of Kansas, Lawrence, Kansas 66045
[12]University of Minnesota, Minneapolis, Minnesota 55455
[13]State University of New York at Albany, Albany, New York 12222
[14]Ohio State University, Columbus, Ohio 43210
[15]University of Oklahoma, Norman, Oklahoma 73019
[16]Purdue University, West Lafayette, Indiana 47907
[17]University of Rochester, Rochester, New York 14627
[18]Stanford Linear Accelerator Center, Stanford University, Stanford, California 94309
[19]Southern Methodist University, Dallas, Texas 75275
[20]Syracuse University, Syracuse, New York 13244
[21]Vanderbilt University, Nashville, Tennessee 37235
[22]Virginia Polytechnic Institute and State University, Blacksburg, Virginia 24061
[23]Wayne State University, Detroit, Michigan 48202
[24]California Institute of Technology, Pasadena, California 91125
[25]University of California, San Diego, La Jolla, California 92093

I. INTRODUCTION

It is important to measure the size of $\mathcal{A}(b \to s\ g^*)$, the amplitude for the gluonic penguin, in order to interpret the CP violating asymmetries which may be observed at future high luminosity facilities. Gluonic penguin modes will also be used to search for direct CP violation.

In accompanying papers, CLEO reports the observation of signals in the exclusive $B^- \to K^- \eta'$ [1] and $\bar{B}^0 \to K^- \pi^+$ [2] modes which are expected to be dominated by the $b \to s\ g^*$ amplitude. Another approach using quasi-inclusive decays could provide additional information on $\mathcal{A}(b \to s\ g^*)$. At the $\Upsilon(4S)$ resonance, quasi two-body decays from $b \to s\ g^*$ can be distinguished from $b \to c$ decays by examination of the inclusive particle momentum spectrum; the $b \to s\ g^*$ decays populate a region that is beyond the kinematic limit for $b \to c$.

The decay $B \to \eta' X_s$, where X_s denotes a particle containing an s quark, is a signature of the gluonic penguin, $b \to sg^*$, with either $g^* \to s\bar{s}$, $g^* \to u\bar{u}$ or $g^* \to d\bar{d}$. To reduce the large background from continuum production of η', we apply the B reconstruction technique which was previously used to isolate an inclusive signal for $b \to s\gamma$ and search for inclusive $B \to X_s\phi$ transitions [3]. It is important to note that other physical processes, $b \to u$ decays with η' mesons and internal spectator $b \to c$ decays such as $\bar{B}^0 \to D^0\eta^{'}$, may also contribute in the high momentum region. These processes may be distinguished by examination of the $M(X_s)$ spectrum, the dE/dx energy loss of the kaon candidate in the X_s system, and ΔE, the difference between the beam energy and the reconstructed energy.

II. EXPERIMENTAL ANALYSIS

The CLEO II detector [4] is designed to measure charged particles and photons with high efficiency and precision. The data sample used in this analysis has an integrated luminosity of 3.1 fb^{-1}. This sample contains about 3.3×10^6 $B\bar{B}$ pairs. Another data sample with an integrated luminosity of 1.6 fb^{-1} was taken at energies about 60 MeV below the $\Upsilon(4S)$ resonance and is used to subtract the non-resonant background. Hadronic events are selected by requiring at least three charged tracks, a total detected energy of at least 0.15 $E_{c.m.}$, and a primary vertex within 5 cm along the beam (z) axis of the interaction point.

Standard track quality requirements are imposed. For the charged kaon candidate we require consistent particle ID using dE/dx. Candidate $\eta^{'}$ mesons are then reconstructed in the $\eta^{'} \to \eta\pi^+\pi^-$, $\eta \to \gamma\gamma$ mode. We use $\gamma\gamma$ combinations with one γ in the good endcap and one in the good barrel or with both photon candidates in the good barrel. The absolute value of the cosine of the η decay angle is required to be less than 0.85 to remove asymmetric decays. The raw $\gamma\gamma$ invariant mass of each η candidate must be within 30 MeV of the nominal η mass. The η candidate is kinematically fitted to the nominal η mass and is then combined with the charged pions to form the $\eta^{'}$ candidate.

Following the method that was used to observe inclusive $b \to s\gamma$ transitions, we form combinations of a charged kaon, an $\eta^{'}$ and n pions where $n \leq 4$ (at most one of these pions is allowed to be neutral). We require that these combinations be consistent in beam-constrained mass (M_B) and energy difference ($\Delta E = E_{observed} - E_{beam}$) with a B meson.

Eight decay modes and their charge conjugates are considered:

1. $B^- \to K^-\eta^{'}$
2. $\bar{B}^0 \to K^-\eta^{'}\pi^+$
3. $B^- \to K^-\eta^{'}\pi^0$
4. $B^- \to K^-\eta^{'}\pi^-\pi^+$
5. $\bar{B}^0 \to K^-\eta^{'}\pi^+\pi^0$
6. $\bar{B}^0 \to K^-\eta^{'}\pi^+\pi^-\pi^+$
7. $B^- \to K^-\eta^{'}\pi^+\pi^-\pi^0$
8. $\bar{B}^0 \to K^-\eta^{'}\pi^+\pi^-\pi^+\pi^0$

In case of multiple entries for a decay mode, we choose the best entry on the basis of a χ^2 formed from M_B, and ΔE. (i.e. $\chi^2 = (M_B/\delta M_B)^2 + (\Delta E/\delta\Delta E)^2$). In case of multiple decay modes per event, the best decay mode candidate is picked on the basis of the same χ^2.

To further reduce the background, we require that the ratio of second to zeroth Fox-Wolfram moments R_2 be less than 0.45. This allows discrimination between the spherical $B\bar{B}$ events and the jet-like continuum background. We also require that $|\cos\theta_B| < 0.95$ where θ_B is the angle between the B meson candidate and the z-axis of the detector. Since B meson pairs are produced with a distribution proportional to $\sin^2\theta_B$, this also gives modest background rejection. We then require that the cosine of the angle between the sphericity axis of the B candidate and the sphericity axis of the remainder of the event satisfy $|\cos(\theta_{spheri})| < 0.6$. This reduces the large continuum background which is concentrated near $\cos(\theta_{spheri}) = \pm 1$, while the expected signal is uniformly distributed in this variable. These cuts are similar to those that were used in previous B reconstruction analyses of $b \to s\gamma$ and $B \to \phi X_s$.

We require $|\Delta E| < 0.1$GeV and $M_B > 5.275$ GeV. To perform the continuum subtraction correctly, the continuum beam-constrained mass must be shifted upwards by the difference between half the continuum center of mass energy and the on-resonance center of mass energy and the η' momentum must also be scaled.

The $\eta\pi^+\pi^-$ mass spectrum in the high momentum window $2.7 > p > 2.0$ GeV/c is then examined. The signal will be excess η' production after continuum subtraction. The final $\eta\pi^+\pi^-$ invariant mass spectrum for the on-resonance and off-resonance samples is shown in Fig. 1.

We find 50.7 ± 8.6 events on the $\Upsilon(4S)$ resonance and 6.1 ± 4.1 off resonance (unscaled). This gives an excess of 39.0 ± 10.3 events. Other ways of determining the yield have been examined. Fitting the continuum-subtracted plot gives 38.4 ± 10.7 events. Using a 2nd order polynomial parameterization rather than a linear parameterization gives a yield of 38.6 ± 11.9. Fitting the continuum-subtracted yield with a second-order polynomial background gives 39.1 ± 11.8 events. These yields are consistent with the yield determined from the fit with a linear background. We estimate a systematic error of 3% from the choice of a fitting function.

The continuum-subtracted distributions of M_B, ΔE and $\cos\theta_{\rm spheri}$ for data with the expectation of a Monte Carlo simulation of quasi two-body $B \to \eta' X_s$ modes superimposed are shown in Figs. 2 (a),(b),(c).

We have calculated the background from all $b \to c$ decay modes included in the CLEO Monte Carlo simulation of B decay, using a simulation with 500 times the luminosity of the CLEO data set. This includes background from processes such as $\bar{B}^0 \to D^+\pi^-$, $D^+ \to \eta'\pi^+$ or $\bar{B}^0 \to D_s^- D^+$, $D_s^+ \to \eta'\pi^+$. Extrapolating to our data sample we obtain an estimated $b \to c$ background of 0.2 events (upper limit). We conclude that the observed excess in high momentum η' production is not consistent with $B\bar{B}$ physics that is already included in the CLEO Monte Carlo simulation of B decay.

In order to determine the efficiency, we generated a number of exclusive $b \to s$ gluon decay modes. The decay modes considered and the efficiencies for the standard cuts in the B reconstruction analysis are given in Table I. For all the background and signal Monte Carlo samples, we force $\eta' \to \eta\pi^+\pi^-, \eta \to \gamma\gamma$. We consider both charged and neutral B decay modes in the efficiencies listed below. It should also be noted that the kaonic resonances $K^{(n)}$ are allowed to decay into all the decay modes allowed by the PDG. The efficiency given in Table I corrects for unobserved modes with K^0 mesons and other decays that are not explicitly reconstructed. The uncertainty in the model of the signal leads to the largest systematic error in the result. It is determined by comparing the detection efficiency determined with varying the weighting of the different modes. This error is 16%. The detection efficiency is averaged over B^0 and B^+ mesons. It should also be noted that no attempt has been made to calculate the branching fraction of the decays that lie outside the η' momentum window between $2.0 - 2.7$ GeV/c.

III. INTERPRETATION OF THE SIGNAL

Approximately 10% of the inclusive yield comes from the exclusive decay mode $B^- \to \eta' K^-$. The signal in this exclusive mode is discussed in detail in an accompanying paper [1]. There is no significant excess in the K^* mass region. The remainder of the yield comes from events with X mass near or above charm threshold. The fitted continuum-subtracted yields are given in Table II.

The possible sources of high momentum η' in B decay are

- $b \to u$ processes such as $B \to \eta' \pi, \eta' \rho, \eta' a_1$;
- $b \to sg^*$;
- color-suppressed $b \to c$: $B \to \eta' D^{0(*)}$, $B \to \eta' X_c^0$ (resonant or non-resonant charm stuff)

The ΔE distribution and dE/dx measurements provide information that can be used to distinguish between $b \to sg^*$ and $b \to u$ processes. The ΔE distributions for $b \to u$ modes ($B \to \eta' \pi / B \to \eta' \rho / B \to \eta' a_1$) are shifted relative to those for $b \to sg^*$ modes such as ($B \to \eta' K n\pi$) due to the difference between the kaon and pion masses. This is shown in Fig. 3(a). The shift in ΔE provides one way to discriminate between $b \to sg^*$ and $b \to u$. In addition, the dE/dx of the kaon candidate distinguishes between $b \to s\ g^*$ and $b \to u$ modes. The discrimination that is provided by particle identification is illustrated in Fig. 3(b).

To maximize the separation between $b \to sg^*$ and $b \to u$, we form a difference of χ^2 between the kaon and pion hypotheses from four quantities: $\Delta E(K)$, $\Delta E(\pi)$ with the kaon assignment changed to the pion hypothesis, $\sigma(\mathrm{dE/dx(K)})$ for the kaon candidate, $\sigma(\mathrm{dE/dx}(\pi))$ for the kaon candidate assigned to the pion hypothesis,

$$\Delta\chi^2 = (\Delta E(K)/\delta\Delta E(K))^2 - (\Delta E(\pi)/\delta\Delta E(\pi))^2 + (\sigma(\mathrm{dE/dx(K)})^2 - \sigma(\mathrm{dE/dx}(\pi))^2.$$

We then fit $\Delta\chi^2$ to the sum of contributions determined from Monte Carlo simulations of $b \to sg^*$ and $b \to u$. To take into account for a small contribution of pions in the η' sideband, a scaled sideband is included as a term in the fit.

From the fit, we find

$$f(b \to sg^*) = 82 \pm 20\% \quad (32.0 \pm 7.8 \text{ events})$$

$$f(b \to u) = 18 \pm 20\% \quad (7.0 \pm 7.8 \text{ events})$$

This demonstrates that an enhancement of $b \to u$ modes with η' mesons can be responsible for at most half of the the observed inclusive η' signal.

It is difficult to differentiate between $b \to sg^*$ and color-suppressed $b \to c$ in the absence of reliable models for both. If one models color-suppressed $b \to c$ with the sum of $\bar{B}^0 \to \eta' D^0$ and $\bar{B}^0 \to \eta' D^{0*}$, then that is not a good representation of the signal. The $\bar{B}^0 \to D^0\eta'$ decay mode peaks at the D mass in the $M(X_s)$ mass distribution, while the $\bar{B}^0 \to D^{*0}\eta'$ mode peaks in the pseudo-D mass distribution obtained by removing the appropriate pion from the X_s system. No such peaks are observed in data as shown in Figure 4. We have evaluated the Kolmogorov-Smirnov confidence levels for several models of color-suppressed decay. For example, the confidence level that the X_s data is due to $D^0\eta'$ is 0.4% while for $D^{*0}\eta'$ it is 0.12%. The confidence level that $D^{**}(2.2)\eta'$ explains the data is 2.7% (where $D^{**}(2.2)$ is a hypothetical broad p-wave meson). We have also considered several combinations of color-suppressed background. For example, an equal mixture of $D^0\eta'$ and $D^{*0}\eta'$ has a confidence level less than 0.05%. A mixture with 20% $D^0\eta'$, 40% $D^{*0}\eta'$ and 40% $D^{**}(2.2)\eta'$ has a confidence level of 0.6%. A similar examination of the pseudo-D mass distribution shows that the probability that $D^{*0}\eta'$ can account for the signal is 0.6%, and $D^{**}(2.2)\eta'$ has a confidence level of 1.2%.

Thus, it is unlikely that color-suppressed background accounts for a large portion of the observed signal. However, we cannot rule out some contribution from other $\bar{B}^0 \to \eta' X_c^0$ modes besides $\bar{B}^0 \to D^0\eta'$ and $\bar{B}^0 \to D^{*0}\eta'$. The branching fraction would have to be enormous ($\mathcal{O}(0.5\%)$) for $\bar{B}^0 \to \eta' X_c^0$ since the detection efficiency is significantly smaller for such modes than for $b \to sg^*$.

The dominant source of systematic error is the uncertainty due to the modeling of the X_s system. Other sources including the choice of background parameterization, and the uncertainty in the tracking and photon detection are much smaller. Assuming an average detection efficiency of 5.5% (appropriate for $b \to sg^*$) we obtain $\mathcal{B}(B \to \eta' X_s) = (6.2 \pm 1.6(stat) \pm 1.3(sys)) \times 10^{-4}$ for $2.0 < p < 2.7$ GeV/c.

IV. THEORETICAL INTERPRETATION

A number of interpretations have been proposed to account for this experimental result. These include: (I) conventional $b \to sq\bar{q}$ operators with constructive interference between the $u\bar{u}, d\bar{d}$, and $s\bar{s}$ components of the η' [5], (II) $b \to c\bar{c}s$ decays enhanced by $c\bar{c}$ content in the η' wavefunction [6], [7], [8], and (III) $b \to sg^*, g^* \to g\eta'$ from the η' QCD anomaly, which also accounts for the large mass of the η' relative to other members of its SU(3) multiplet [9], [10]. Each of these theoretical scenarios should lead to a characteristic X_s mass spectrum and other distinctive features. For example, the first two scenarios will give a X_s mass distribution peaked near 1.5 GeV while the third scenario gives a three body $gs\bar{q}$ X_s mass spectrum which peaks above 2 GeV. The third scenario appears to be most consistent with the distribution observed in the X_s spectrum of data.

V. CONCLUSION

We have observed a signal for quasi-inclusive $B \to \eta' X$ production. We have shown that it is unlikely that a large part of the yield is from color-suppressed B decay or from $b \to u$ decay modes. The possibility that the signal is due to charmless $b \to s$ processes is consistent with all the features observed in data although other interpretations cannot be completely ruled out. Given the $b \to sg^*$ interpretation, the branching ratio is $\mathcal{B}(B \to \eta' X_s) = (6.2 \pm 1.6(stat) \pm 1.3(sys)) \times 10^{-4}$ for $2.0 < p < 2.7$ GeV/c.

VI. ACKNOWLEDGMENTS

We gratefully acknowledge the efforts of the CESR staff in providing us with excellent luminosity. This work was supported by the National Science Foundation, the U.S. Department of Energy, the Heisenberg Foundation, the Alexander von Humboldt Stiftung, Research Corporation, the Natural Sciences and Engineering Research Council of Canada, and the A.P. Sloan Foundation.

REFERENCES

[1] CLEO Collaboration, submission to this conference, EPS333.

[2] CLEO Collaboration, submission to this conference, EPS334.

[3] M. S. Alam *et al* [CLEO Collaboration], Phys. Rev. Lett. **74**, 2885 (1995).

[4] Y. Kubota *et al* [CLEO Collaboration], Nucl. Instrum. Methods Phys. Res. A **320**, 66 (1992)

[5] H.J. Lipkin, Phys. Lett. B. 254, 247 (1991).

[6] K. Berkelman, CLEO internal note and private communication.

[7] I. Halperin and A. Zhitnitsky, hep-ph/9704412; I. Halperin and A. Zhitnitsky, hep-ph/9705251; E. Shuryak and A. Zhitnitsky, hep-ph/9706316.

[8] F. Yuan and K-T. Chao, hep-ph/9706294.

[9] D. Atwood and A. Soni, hep-ph/9704357.

[10] W-S. Hou and B. Tseng, hep-ph/9705304.

TABLE I. Detection efficiency for $B \to \eta' X_s$ modes

Mode	ϵ(detection and reconstruction)
$B \to K\eta'$	0.076 ± 0.006
$B \to K^*(892)\eta'$	0.058 ± 0.005
$B \to K_1(1270)\eta'$	0.050 ± 0.005
$B \to K_1^*(1406)\eta'$	0.053 ± 0.005
$B \to K_2^*(1429)\eta'$	0.051 ± 0.005
$B \to K_3^*(1774)\eta'$	0.046 ± 0.005
$B \to K_4^*(2200)\eta'$	0.046 ± 0.005
Equal mixture of exclusive modes	0.055 ± 0.003
$B \to \eta' s\bar{d} + B \to \eta' s\bar{u}$ (JETSET hadronization)	0.055 ± 0.003

TABLE II. Yield as a function of $M(X_s)$ for $B \to \eta' X_s$

$M(X_s)$ (GeV) Range	N (on)	N(off)	Yield
$0.4 < M(X) < 0.6$	4	0	4
$0.6 < M(X) < 1.2$	2.7 ± 2.1	0.6 ± 1.1	2.1 ± 2.9
$1.2 < M(X) < 1.8$	18.0 ± 4.9	6.6 ± 3.2	11.4 ± 7.6
$1.8 < M(X) < 2.5$	26.0 ± 6.4	-0.8 ± 2.3	26.8 ± 7.8

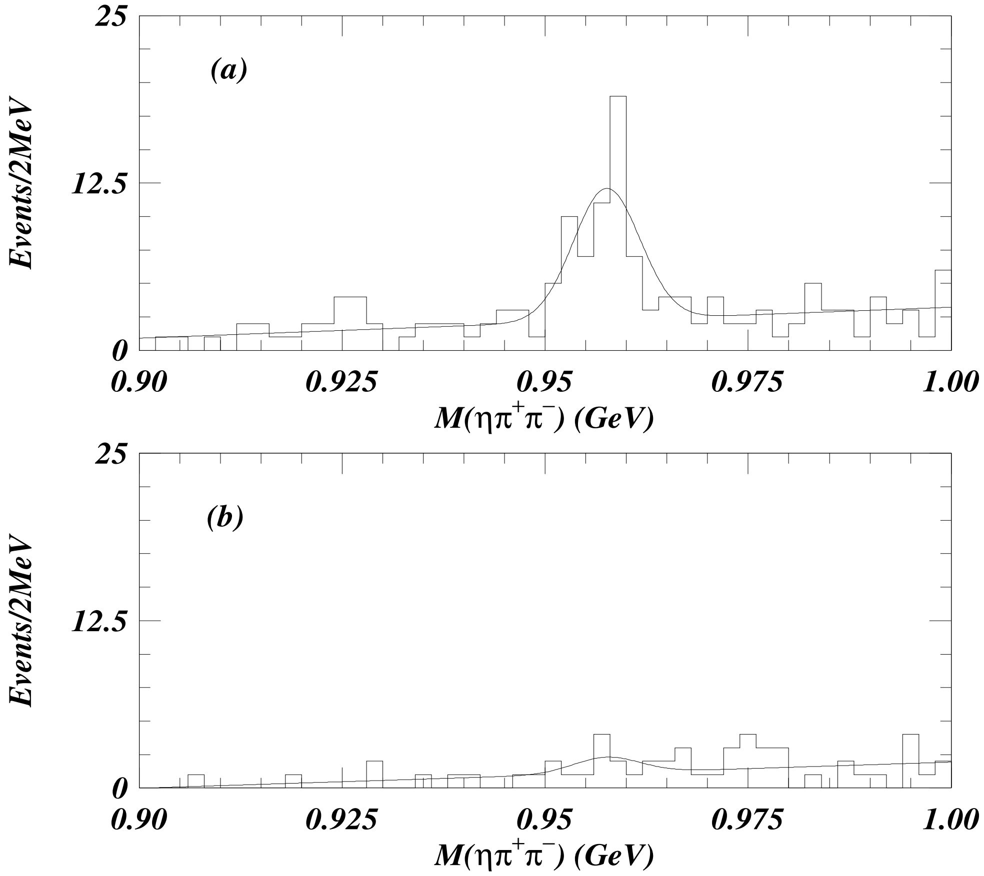

FIG. 1. The distribution of $\eta\pi^+\pi^-$ mass for (a) on-resonace data and (b) below-resonance data

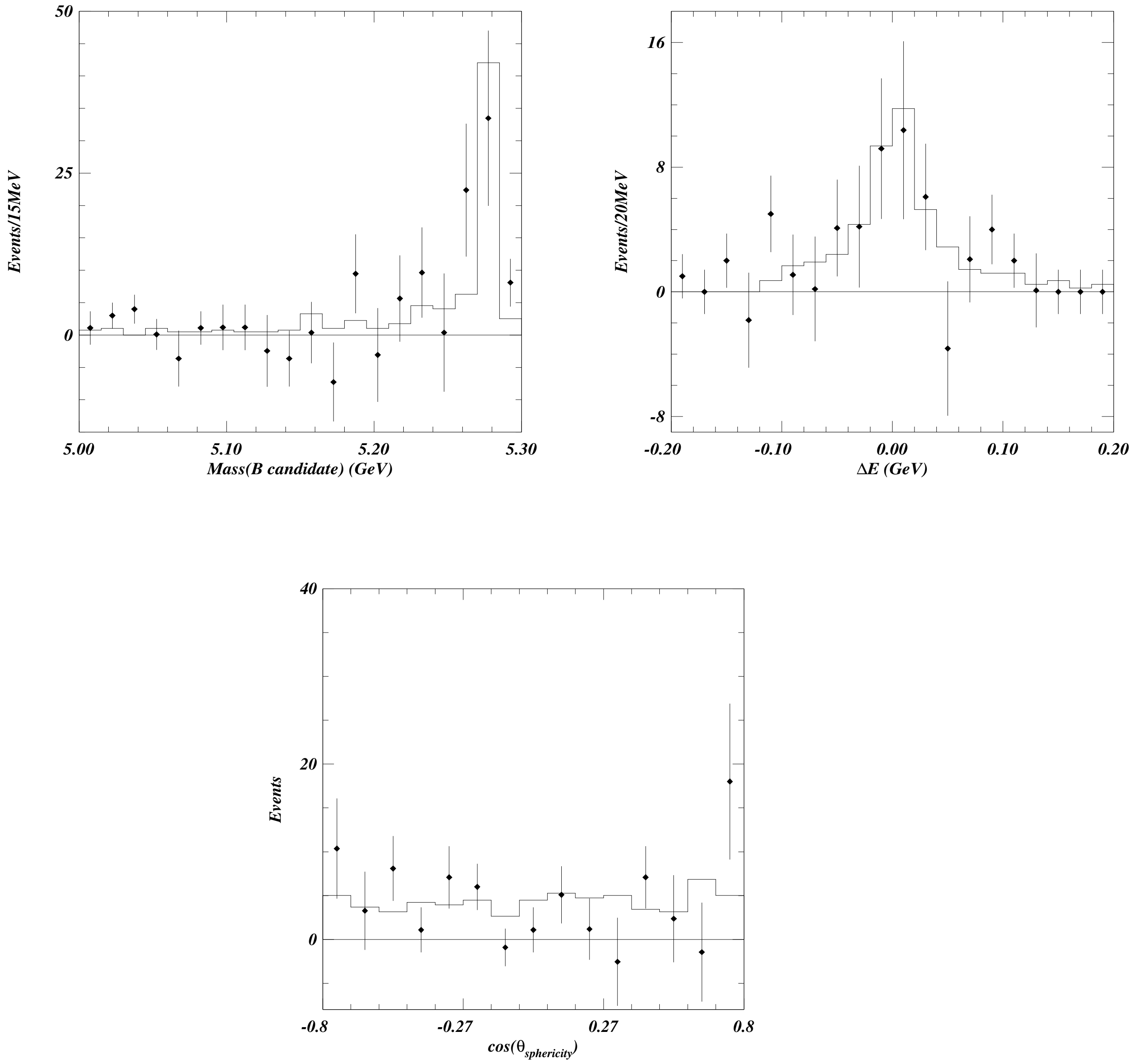

FIG. 2. The continuum subtracted distributions of (a) beam constrained mass (b) ΔE and (c) the cosine of the sphericity angle. The solid histograms are the expected distribution from a Monte Carlo simulation of exclusive two body $b \to sg^*$ decays.

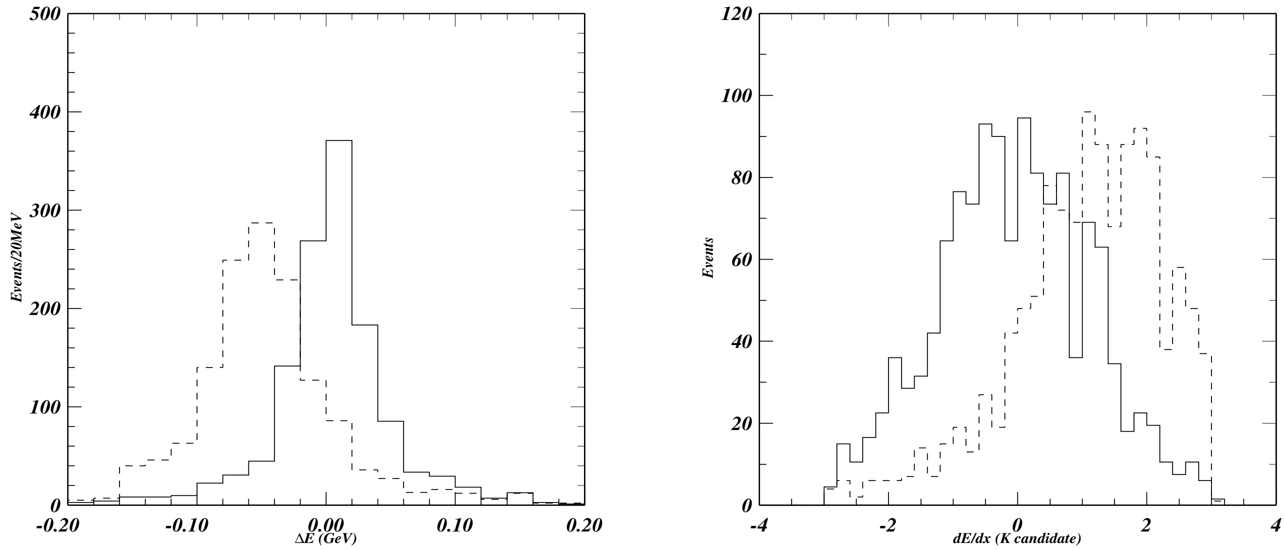

FIG. 3. The expected distributions of (a) ΔE (b) dE/dx for the kaon candidate for Monte Carlo $b \to sg^*$ (solid) and $b \to u$ (dashed).

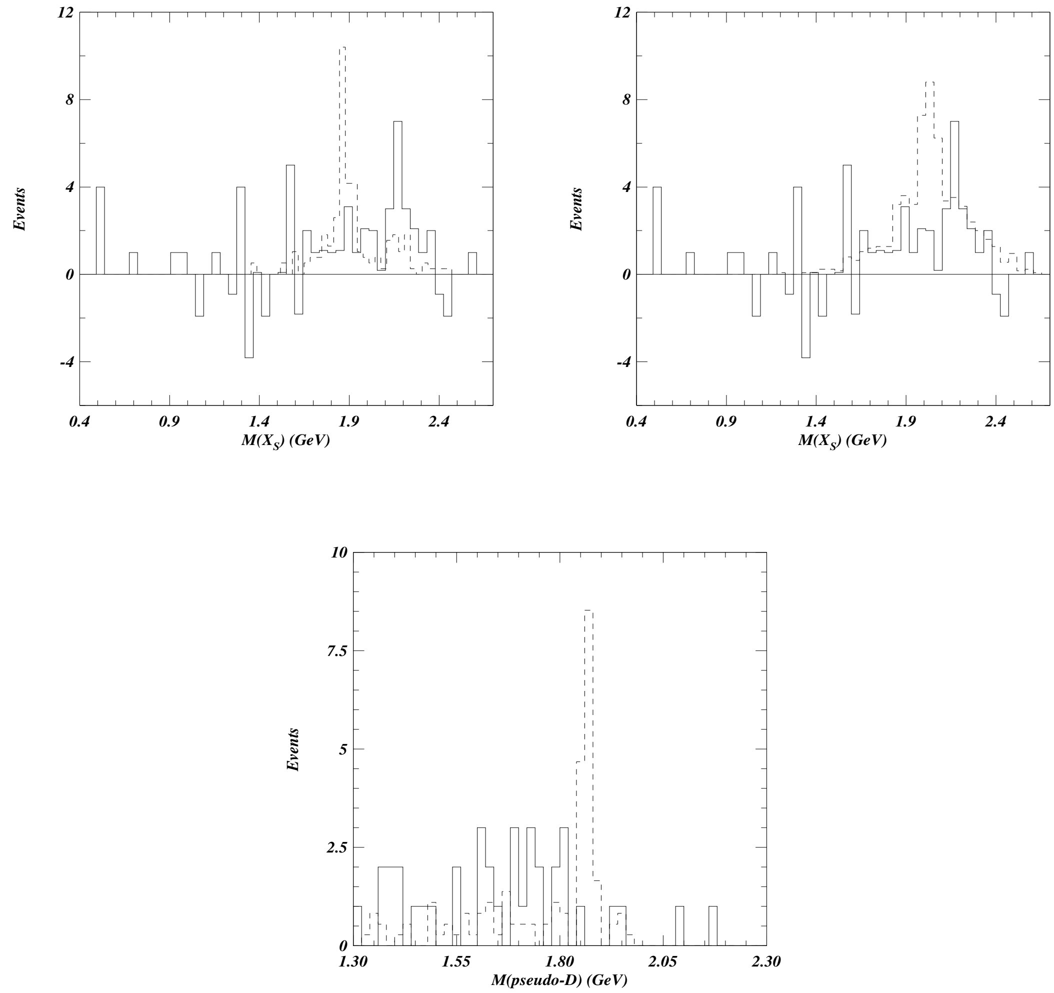

FIG. 4. The X_s mass distribution (solid) with expected X_s distribution (dashed) for (a) $\bar{B}^0 \to D^0\eta'$ and (b) $\bar{B}^0 \to D^{*0}\eta'$ are shown in (a) and (b). The distribution of pseudo-D mass (solid) with the expectation from $\bar{B}^0 \to D^{*0}\eta'$ (dashed) is shown in (c).